Methods of digital holography: a comparison

Thomas Kreis, Mike Adams, Werner Jueptner

Thomas M. Kreis, Mike Adams, Werner P. O. Jueptner, "Methods of digital holography: a comparison," Proc. SPIE 3098, Optical Inspection and Micromeasurements II, (17 September 1997); doi: 10.1117/12.281164

SPIE.

Event: Lasers and Optics in Manufacturing III, 1997, Munich, Germany

Invited Paper

Methods of Digital Holography: A Comparison

Thomas M. Kreis, Mike Adams, Werner P. O. Jüptner
BIAS - Bremer Institut für angewandte Strahltechnik
Klagenfurter Str. 2, D 28359 Bremen, Germany

ABSTRACT

Optically generated holograms can be recorded on CCD-arrays if the sampling theorem is obeyed. The digitized and quantized holograms are processed digitally for the reconstruction of intensity and phase of the real or virtual image. This digital reconstruction consists in a numerical realization of the diffraction integral. One approach is the Fresnel approximation employing a single Fourier transform, the other is the interpretation of the diffraction formula as a convolution integral and calculation of this convolution by a double or triple Fourier transform. In this convolution approach the impulse response of free space propagation has to be defined which is then Fourier transformed or the free space transfer function is defined immediately. Impulse response as well as transfer function can be defined exactly or in an approximated version. The main difference between the Fresnel and the convolution approach is the different size of the resulting images. Furthermore in the Fresnel case this size depends on the wavelength and the distance of the object from the CCD, in the other case it does not. In this paper consequences on the reconstructed wavefields and on the interference phase distributions of holographic interferometry are indicated and demonstrated by experimental results.

Keywords: Holography, interferometry, holographic interferometry, digital holography, numerical methods, digital optics, CCD-arrays, diffraction, Fresnel transform, convolution

1 INTRODUCTION

Holography is a method to record and reconstruct optical wave fields. Perhaps the most important application of holography in metrology is holographic interferometry, where wavefields before and after a variation are compared interferometrically. Deformation fields or refractive index variations are coded into macroscopic interference fringes [1]. For precision measurements the reconstructed interference patterns are recorded by a digital TV-camera and evaluated numerically. By methods like fringe tracking, phase-shifting, Fourier transform evaluation, or heterodyning, first the interference phase distribution is determined, from which in a second step the displacement vector fields, strains, stresses, refractive index fields, and related physical quantities can be calculated. One drawback of this procedure is the time consuming optical recording of the holograms onto photoplates or photothermoplastic film, development, repositioning, and optical reconstruction. Therefore a digital recording of the primary holograms and a numerical reconstruction of the complex wavefields from the recorded intensity fields would offer real advantages to holographic metrology.

This paper deals with the methods of numerical evaluation of digitally recorded holograms. After a short outline of some holographic methods and the requirements given by the sampling theorem, a description of digital holographic reconstruction based on diffraction theory is given. Some numerical algorithms to compute the diffraction integral are introduced. The typical features and capabilities of the procedures are identified and compared. Digital holography in this sense is complementary to computer generated holography or synthetic holography, also sometimes called digital holography. While in our case optically generated holograms are digitally recorded and reconstructed, in synthetic holography wavefields from numerically generated holograms are optically reconstructed.

2 HOLOGRAPHIC METHODS

The attempts to use the targets of electronic TV-cameras as recording media for holograms have first resulted in the electronic or digital speckle pattern interferometry (ESPI or DSPI) [2, 3], later in the digital Fresnel holography [4, 5], and the digital Fraunhofer holography [6].

SPIE Vol. 3098 • 0277-786X/97/$10.00

In ESPI/DSPI the object surface is focused onto the camera target and a co-linear reference wave is superposed, Fig. 1 a. The resulting speckle pattern is stored electronically. The speckle pattern after deformation of the object surface is subtracted from the stored one. Thus a severely speckled interference pattern related to the surface deformation field is produced. ESPI or DSPI is image plane holography with interferometric evaluation on an intensity correlation basis. In Fraunhofer holography the far-field diffraction pattern of the wave field reflected from the surface is used, Fig. 1 b, while in Fresnel holography the field in the Fresnel diffraction region is utilized, Fig. 1 c. Since Fresnel holography is the more general one of the two methods, containing Fraunhofer holography as the special case with infinite distance, in the following Fresnel holography is considered. The reference waves in Figs. 1 b and 1 c are collimated waves impinging normally onto the CCD-target. With such reference waves the numerical evaluation is straightforward, as will become obvious in the next sections.

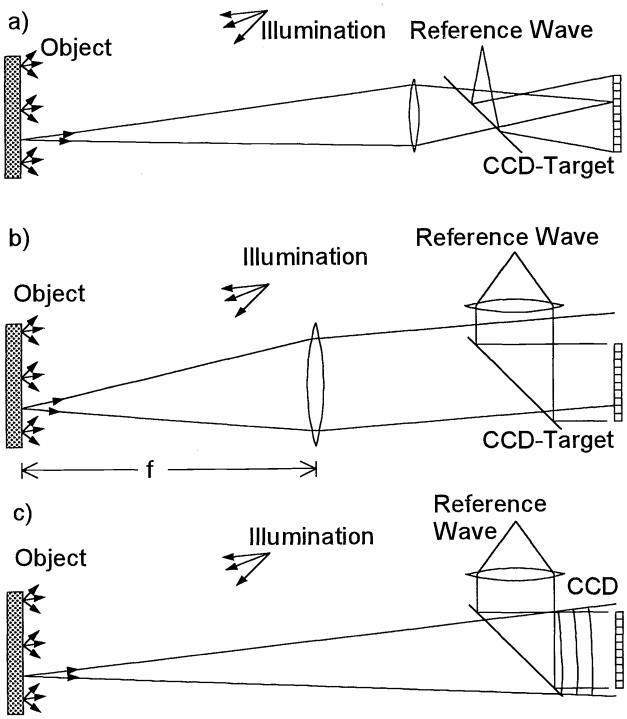

Figure 1: Optical arrangements for a) ESPI/DSPI, b) Fraunhofer holography, c)Fresnel holography

The geometry for the description of digital Fresnel holography is shown in Fig. 2. Without loss of generality we assume a plane rough surface in the (x, y)-plane, that reflects the wave field $b(x, y)$, keeping in mind, that the procedures also apply to nonplane surfaces, or to particle fields. Let the hologram, or the CCD-target resp., be in the (ξ, η)-plane at distance d from the object surface. The reconstructed real image is in the (x', y')-plane, which is at distance d' from the hologram plane.

The microinterference in the hologram at each point is determined by the angle θ between reference wave and object wave by

$$\delta = \frac{\lambda}{2\sin(\theta/2)} \tag{1}$$

where δ is the resulting fringe spacing and λ denotes the used wavelength. For a CCD-array with pixel spacing $\Delta\xi$

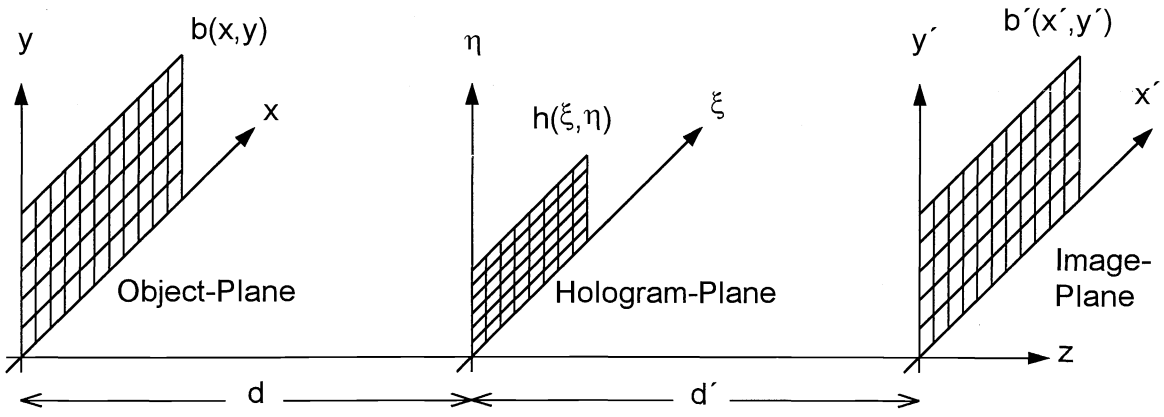

Figure 2: Geometry of digital Fresnel holography

the sampling theorem requires at least two pixels per fringe period $2\Delta\xi < \delta$ or

$$\theta < \frac{\lambda}{2\Delta\xi} \tag{2}$$

since for the small θ we have $\sin\theta \approx \tan\theta \approx \theta$. The small angles θ required by the sampling theorem have to be obtained by a small object size, by objects placed at far distances from the CCD-array, or by an optical demagnification of the wave field by a negative lens [7].

The reference waves used in digital holography may be collimated or divergent, with normal or oblique incidence onto the CCD-array. The one best suited for the numerical evaluation is the plane wave impinging normally with spatially constant amplitude and phase. Up to a real factor it can be modeled by $r(\xi,\eta) = 1 + 0i$.

Hitherto, optical reconstruction was performed by illuminating the developed hologram with the reference wave. So now we multiply the digital hologram with the reference wave field in the hologram plane and calculate the diffraction pattern in the image plane. This complex field represents the real image, if $d' = d$, or the virtual image, if we take $d' = -d$.

The diffracted field in the image plane is given by the Rayleigh-Sommerfeld diffraction formula [8]

$$b'(x',y') = \frac{1}{i\lambda}\int\int h(\xi,\eta)r(\xi,\eta)\frac{\exp\{ik\rho\}}{\rho}\cos\Theta d\xi\ d\eta \tag{3}$$

with

$$\rho = \sqrt{d'^2 + (\xi - x')^2 + (\eta - y')^2} \tag{4}$$

Here $h(\xi,\eta)$ is the recorded hologram, $r(\xi,\eta)$ is the reference wave field, $k = 2\pi/\lambda$ is the wave number, and $\cos\Theta$ is an obliquity factor which normally can be set $\cos\Theta = 1$ due to the small angles between the hologram normal and the rays from the hologram to the image points.

3 FRESNEL-APPROXIMATION

While in (3) the ρ in the denominator can be replaced by d', as long as d' is large compared to $(\xi - x')$ and $(\eta - y')$, ρ in the numerator defines a spatially rapidly varying phase. The same replacement in the numerator therefore would cause inacceptable errors. The Fresnel-approximation uses the binomial expansion $\sqrt{1-a} = 1 + \frac{1}{2}a - \frac{1}{8}a^2 + -\ldots$ for the square root (4), which is valid for small a. Retaining the first two terms, we achieve

$$\rho \approx d'\left[1 + \frac{1}{2}\left(\frac{\xi - x'}{d'}\right)^2 + \frac{1}{2}\left(\frac{\eta - y'}{d'}\right)^2\right] \tag{5}$$

The diffraction integral (3) now reads

$$\begin{aligned} b'(x',y') &= \frac{1}{i\lambda d'}\int\int h(\xi,\eta)r(\xi,\eta)\exp\left\{ikd'\left[1 + \frac{1}{2}\left(\frac{\xi - x'}{d'}\right)^2 + \frac{1}{2}\left(\frac{\eta - y'}{d'}\right)^2\right]\right\} d\xi\ d\eta \\ &= \frac{\exp\{ikd'\}}{i\lambda d'}\int\int h(\xi,\eta)r(\xi,\eta)\exp\left\{\frac{ik}{2d'}\left[(\xi - x')^2 + (\eta - y')^2\right]\right\} d\xi\ d\eta \\ &= \frac{\exp\{ikd'\}\exp\{i\pi d'\lambda(\nu^2 + \mu^2)\}}{i\lambda d'}\int\int h(\xi,\eta)r(\xi,\eta)\exp\left\{\frac{i\pi}{d'\lambda}(\xi^2 + \eta^2)\right\}\exp\{-2i\pi(\xi\nu + \eta\mu)\}d\xi\ d\eta \end{aligned} \tag{6}$$

with $\nu = \frac{x'}{d\lambda}$ and $\mu = \frac{y'}{d\lambda}$. The last line of (6) shows, that the diffracted field is the Fourier transform of the hologram multiplied by the reference wave and the chirp function $\exp\left\{\frac{i\pi}{\lambda d'}(\xi^2 - \eta^2)\right\}$. The result of this Fourier transform is multiplied by a phase factor and the spatially constant intensity factor $1/(i\lambda d')$.

For a numerical evaluation the discrete finite form of (6) is taken, omitting the spatially constant factors. The discretization is given by the CCD-array:

$$b'(n,m) = \exp\left\{-\frac{i\pi d'\lambda}{N^2}\left(\frac{n^2}{\Delta\xi^2}+\frac{m^2}{\Delta\eta^2}\right)\right\}\sum_{k=0}^{N-1}\sum_{l=0}^{N-1} h(k\Delta\xi,l\Delta\eta)r(k\Delta\xi,l\Delta\eta)\exp\left\{\frac{i\pi}{d'\lambda}(k^2\Delta\xi^2+l^2\Delta\eta^2)\right\} \times \exp\left\{2i\pi\left(\frac{kn}{N}+\frac{lm}{N}\right)\right\} \quad (7)$$

or shortly

$$b' = z\cdot\mathcal{F}^{-1}\{h\cdot r\cdot w\} \quad (8)$$

In these equations $h(k\Delta\xi,l\Delta\eta)$ denotes the quantized and digitized hologram, $r(k\Delta\xi,l\Delta\eta)$ is the reference wave, $w(k\Delta\xi,l\Delta\eta) = \exp\left\{\frac{i\pi}{d'\lambda}(k^2\Delta\xi^2+l^2\Delta\eta^2)\right\}$ is the two-dimensional discrete chirp function and $z(n\Delta x',m\Delta y') = \exp\left\{-\frac{i\pi d'\lambda}{N^2}\left(\frac{n^2}{\Delta\xi^2}+\frac{m^2}{\Delta\eta^2}\right)\right\} = \exp\left\{-\frac{i\pi}{d'\lambda}\left(n^2\Delta x'^2+m^2\Delta y'^2\right)\right\}$.

The pixel size in the reconstructed image is

$$\Delta x' = \frac{d'\lambda}{N\Delta\xi} \qquad \Delta y' = \frac{d'\lambda}{N\Delta\eta} \quad (9)$$

where N is the pixel number of the CCD-array in each direction.

In most applications the phase factor $z(n\Delta x',m\Delta y')$ can be neglected, as is the case if only the intensities of the reconstruction are of interest, or if phase differences matter, as in holographic interferometry. z is independent of the evaluated hologram, thus at each point it gives the same phase shift in all reconstructions of different object states and cancels out in the phase-subtraction process of holographic interferometry.

A typical example is shown in Fig. 3. The hologram of a die placed $1.054m$ apart from the CCD-array of $N\times N =$

a) b)

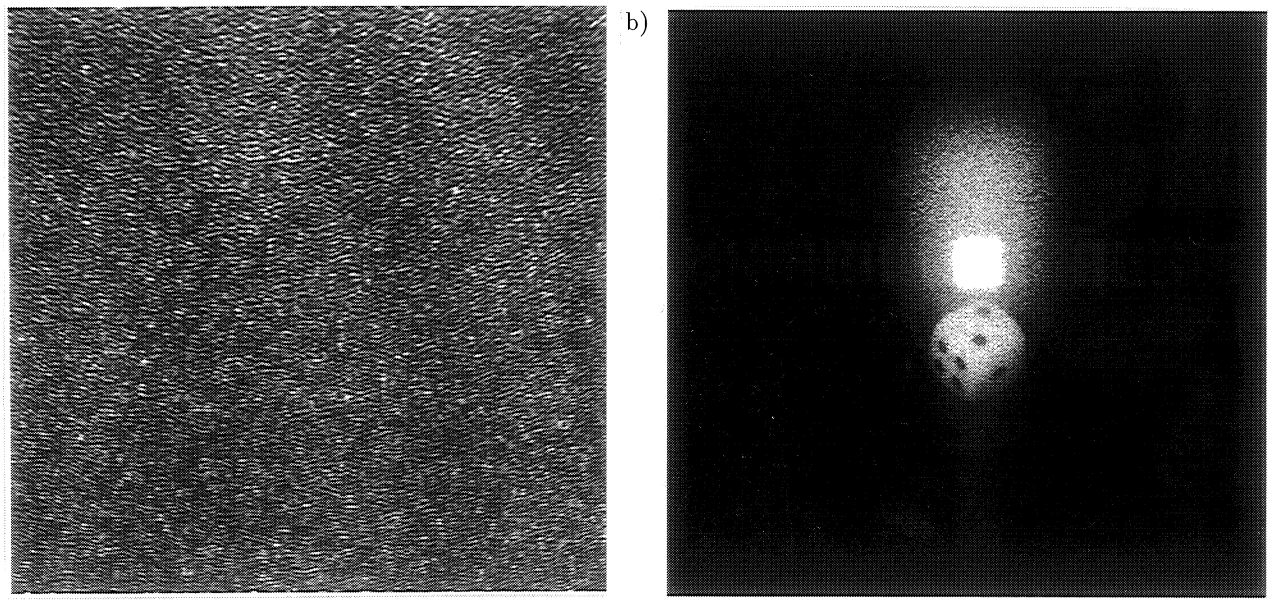

Figure 3: Hologram (a) and digitally reconstructed intensity (b) of a die

1024×1024 pixels with pixel size $\Delta\xi = \Delta\eta = 6.8\mu m$ and a wavelength $\lambda = 0.6328\mu m$ is given in Fig. 3 a. The reference wave was a collimated normally impinging one, which is modeled up to a real proportionality constant by $r(k\Delta\xi,l\Delta\eta) = 1.+0.i$. The intensity of the numerically reconstructed complex wavefield is displayed in Fig. 3 b. The high intensity d.c.-term of the Fresnel transform covering the central area of the reconstructed field can be eliminated by the methods described in [9].

4 THE DIFFRACTION INTEGRAL AS A CONVOLUTION

The Rayleigh-Sommerfeld diffraction formula (3) for reconstruction of the wave field $b'(x', y')$ is a superposition integral

$$b'(x', y') = \int\int h(\xi, \eta) r(\xi, \eta) g(x', y', \xi, \eta) d\xi \, d\eta \tag{10}$$

where the impulse response $g(x', y', \xi, \eta)$ is given explicitly by

$$\begin{aligned} g(x', y', \xi, \eta) &= \frac{1}{i\lambda} \frac{\exp\{ik\rho\}}{\rho} \cos\Theta \\ &= \frac{d'}{i\lambda} \frac{\exp\left\{ik\sqrt{d'^2 + (\xi - x')^2 + (\eta - y')^2}\right\}}{d'^2 + (\xi - x')^2 + (\eta - y')^2} \end{aligned} \tag{11}$$

Here $\cos\Theta = d'/\rho$ was used. The second line of (11) shows that the linear system characterized by $g(x', y', \xi, \eta) = g(x' - \xi, y' - \eta)$ is space-invariant: the superposition integral is a convolution. This allows an economic calculation of the diffraction integral without approximation. The convolution theorem states that the Fourier transform of the convolution of $h \cdot r$ with g is the product of the individual transforms $\mathcal{F}\{h \cdot r\}$ and $\mathcal{F}\{g\}$. So $b'(x', y')$ can be calculated by first Fourier transforming $h \cdot r$, then multiplying with the Fourier transform of g, and taking an inverse Fourier transform of this product. The whole process requires at all three Fourier transforms, for which the efficient FFT-algorithm can be employed.

The numerical realization of the impulse response is

$$g(k, l) = \frac{1}{i\lambda} \frac{\exp\left\{\frac{2i\pi}{\lambda}\sqrt{d'^2 + (k - N/2)^2\Delta\xi^2 + (l - N/2)^2\Delta\eta^2}\right\}}{\sqrt{d'^2 + (k - N/2)^2\Delta\xi^2 + (l - N/2)^2\Delta\eta^2}} \tag{12}$$

The shift of the coordinates by $N/2$ is on symmetry reasons. Furthermore the intensity term $\cos\Theta = d'/\rho$ has been neglected, since for the θ required by (2) the resulting $\cos\Theta$ differs by less than 1/1000 from 1. Formula (12) represents the impulse response function of free space propagation.

The Fourier transform of the impulse response $g(k, l)$ is the transfer function $G(n, m)$. Thus according to the transfer function of free space propagation we also may define directly

$$G(n, m) = \exp\left\{\frac{2\pi i d'}{\lambda}\sqrt{1 - \frac{\lambda^2\left(n + \frac{N^2\Delta\xi^2}{2d'\lambda}\right)^2}{N^2\Delta\xi^2} - \frac{\lambda^2\left(m + \frac{N^2\Delta\eta^2}{2d'\lambda}\right)^2}{N^2\Delta\eta^2}}\right\} \tag{13}$$

and at least we save one Fourier transform.

An examination of the first line of (6) shows that in a like manner the Fresnel-transform is a convolution, with the impulse response

$$g_F(\xi - x', \eta - y') = \frac{\exp\{ikd'\}}{i\lambda d'} \exp\left\{\frac{i\pi}{\lambda d'}\left[(\xi - x')^2 + (\eta - y')^2\right]\right\} \tag{14}$$

The Fresnel approximation of the transfer function is

$$G_F(n, m) = \exp\left\{i\pi d'\left[\frac{2}{\lambda} - \lambda\left(\frac{n}{N\Delta\xi} + \frac{N\Delta\xi}{2d'\lambda}\right)^2 - \lambda\left(\frac{m}{N\Delta\eta} + \frac{N\Delta\eta}{2d'\lambda}\right)^2\right]\right\} \tag{15}$$

The pixel size in the reconstructed image, when reconstructing via the multiplication with the transfer function in the spatial frequency domain, is

$$\Delta x' = \Delta\xi \qquad \Delta y' = \Delta\eta \tag{16}$$

The resulting image covers the area $N\Delta\xi \times N\Delta\eta$ of the scene instead of $\frac{d'\lambda}{\Delta\xi} \times \frac{d'\lambda}{\Delta\eta}$ for the Fresnel transform. The larger image size in the latter case (as long as $d' > \Delta\xi^2/\lambda$) shows that there is even more information coded in the hologram than is reconstructed by a single convolution integral.

There is no way to extract this additional information by fixing different scales to the (ξ, η)- and (x', y')-planes. This would violate the space invariance, which is a necessary condition for the validity of the convolution theorem. However, a shift in one plane retains the space invariance. Therefore the application of the impulse response

$$g(k + s_k, l + s_l) = \frac{1}{i\lambda} \frac{\exp\left\{\frac{2i\pi}{\lambda}\sqrt{d'^2 + (k - N/2 + s_k)^2\Delta\xi^2 + (l - N/2 + s_l)^2\Delta\eta^2}\right\}}{\sqrt{d'^2 + (k - N/2 + s_k)^2\Delta\xi^2 + (l - N/2 + s_l)^2\Delta\eta^2}} \tag{17}$$

shifts the reconstructed field by $(s_k\Delta\xi, s_l\Delta\eta)$. A limit to possible shifts (s_k, s_l) is only given by the sampling theorem

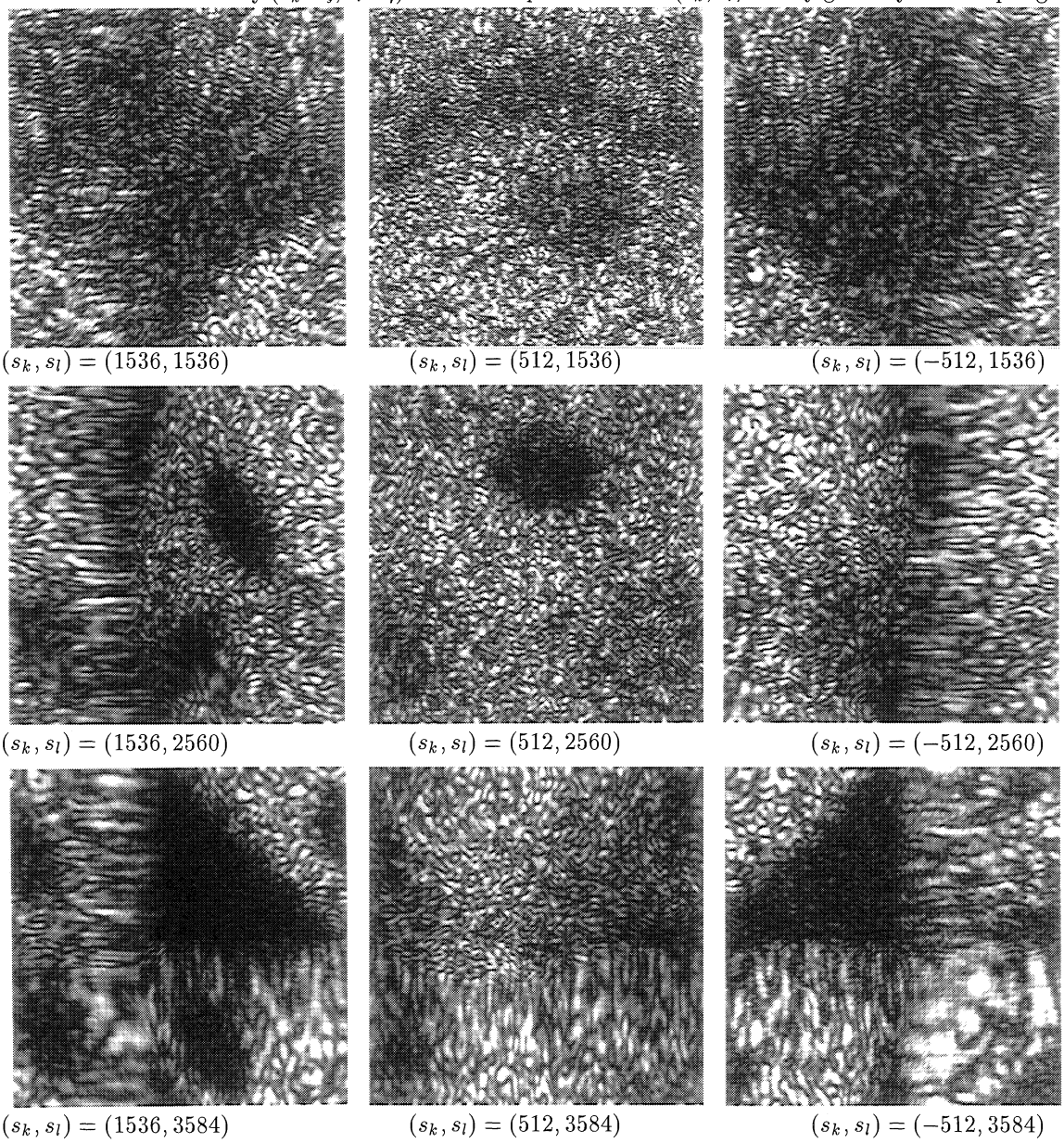

Figure 4: Reconstructions by the convolution approach for different image shifts

(2). In Fig. 4 we see the reconstructions for 9 different shifts. A comparison with Fig. 3 clearly shows the different image size compared to the Fresnel evaluation.

Even a scaling of the image is possible, as long as the same scaling is performed in the (ξ, η)- and (x', y')-planes. So

we may add black pixels at the margins to expand the $N \times N$-pixel hologram to a $2N \times 2N$-pixel hologram: The central $N \times N$ pixels stem from the original hologram, the surrounding pixels carry the intensity 0. The reconstructed image has the size $2N\Delta\xi \times 2N\Delta\eta$. An example is given in Fig. 5, where Fig. 5 a shows the augmented hologram and Fig. 5 b the corresponding reconstruction.

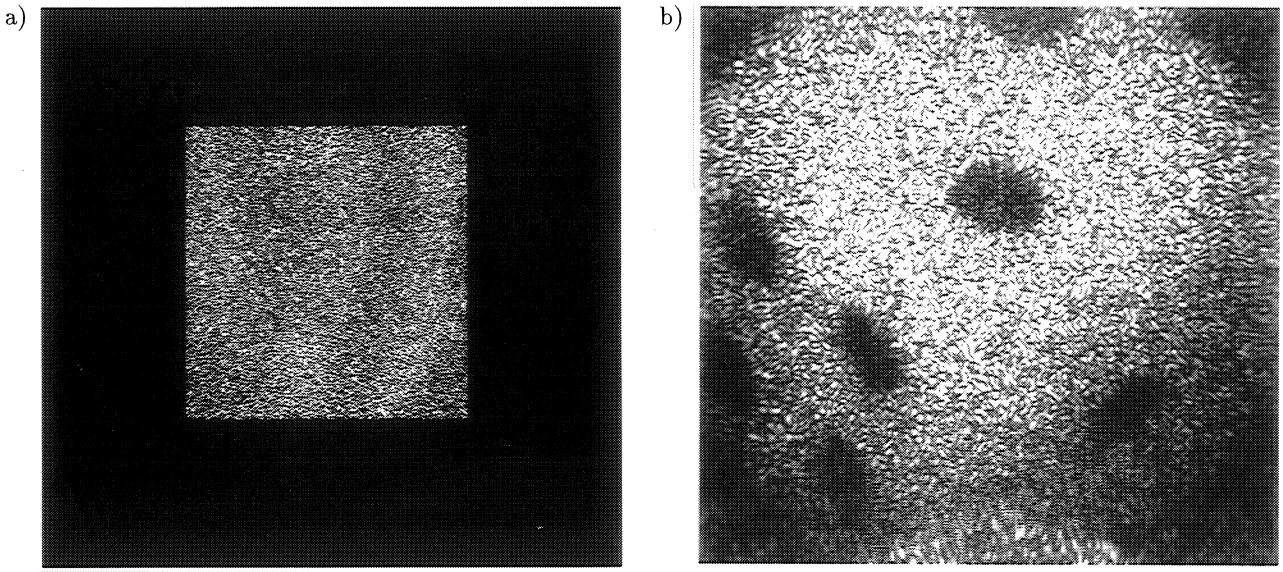

Figure 5: Augmented hologram (a) and image (b) reconstructed by the convolution approach

Alternatively we can average the intensities of four neighboring pixels in the hologram and in this way build the central $N/2 \times N/2$ pixels of an $N \times N$-pixel hologram. Again the surrounding pixels have zero intensity. The result is an $N \times N$-pixel image with $\Delta x' = 2\Delta\xi$ and $\Delta y' = 2\Delta\eta$. These approaches can be combined as shown in Fig. 6. Fig. 6 a displays the averaged and augmented digital hologram, now containing 2048×2048 pixels of size$(13.6\mu m)^2$.

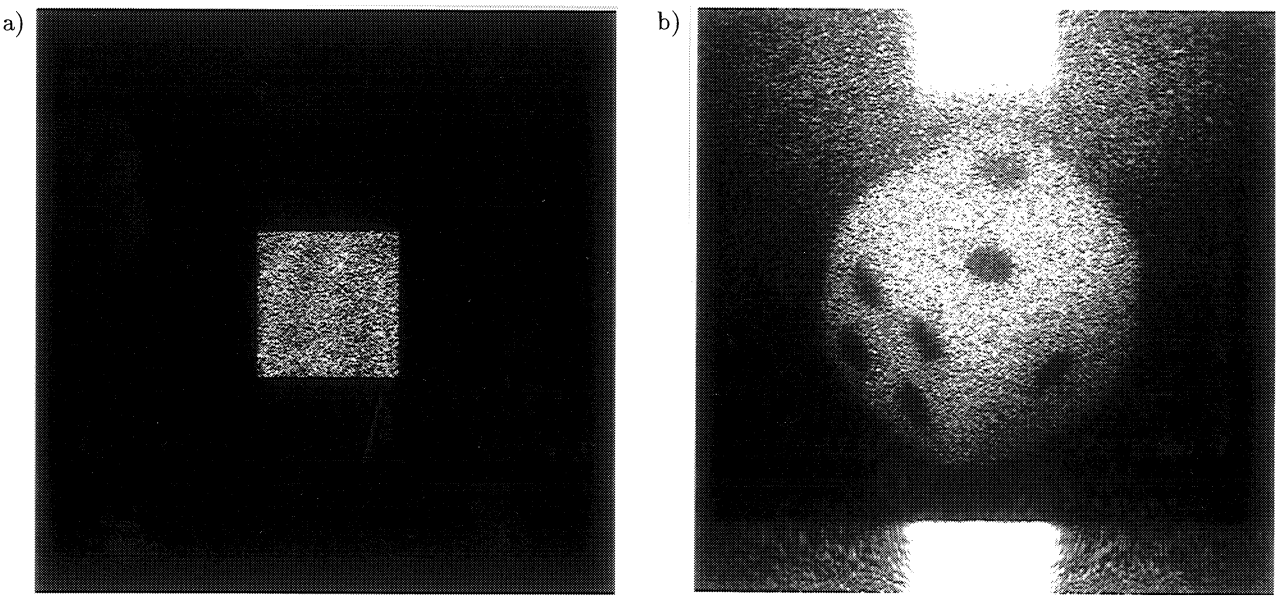

Figure 6: Augmented and averaged hologram (a) and image (b) reconstructed by the convolution approach

The intensity of the resulting wavefield is shown in Fig. 6 b. Of course other factors than the demonstrated doubling are feasible as well.

5 COMPARISON OF THE RECONSTRUCTION METHODS

The different realizations of the diffraction integral are summarized in the following table.

Method	Algorithm	Impulse Response/Transfer function
Fresnel-Approxi. (Chirp function)	$z \cdot \mathcal{F}^{-1}\{h \cdot r \cdot w\}$	$w(k,l) = \exp\left\{\frac{i\pi}{d'\lambda}(k^2\Delta\xi^2 + l^2\Delta\eta^2)\right\}$ $z(n,m) = \exp\left\{\frac{-i\pi d'\lambda}{N^2}(\frac{n^2}{\Delta\xi^2} + \frac{m^2}{\Delta\eta^2})\right\}$
Fresnel-Approxi. (Impulse response)	$\mathcal{F}^{-1}\{\mathcal{F}\{h \cdot r\} \cdot \mathcal{F}\{g_F\}\}$	$g_F(k,l) = \frac{\exp\{id'2\pi/\lambda\}}{i\lambda d'} \exp\left\{\frac{i\pi}{\lambda d'}\left[(k-N/2)^2\Delta\xi^2 + (l-N/2)^2\Delta\eta^2\right]\right\}$
Fresnel-Approxi. (Transfer function)	$\mathcal{F}^{-1}\{\mathcal{F}\{h \cdot r\} \cdot G_F\}$	$G_F(n,m) = \exp\left\{i\pi d'\left[\frac{2}{\lambda} - \lambda\left(\frac{n}{N\Delta\xi} + \frac{N\Delta\xi}{2d'\lambda}\right)^2 - \lambda\left(\frac{m}{N\Delta\eta} + \frac{N\Delta\eta}{2d'\lambda}\right)^2\right]\right\}$
Diffraction integral (Impulse response)	$\mathcal{F}^{-1}\{\mathcal{F}\{h \cdot r\} \cdot \mathcal{F}\{g\}\}$	$g(k,l) = \frac{1}{i\lambda} \frac{\exp\left\{\frac{2\pi i}{\lambda}\sqrt{d'^2+(k-N/2)^2\Delta\xi^2+(l-N/2)^2\Delta\eta^2}\right\}}{\sqrt{d'^2+(k-N/2)^2\Delta\xi^2+(l-N/2)^2\Delta\eta^2}}$
Diffraction integral (Transfer function)	$\mathcal{F}^{-1}\{\mathcal{F}\{h \cdot r\} \cdot G\}$	$G(n,m) = \exp\left\{\frac{2\pi i d'}{\lambda}\sqrt{1 - \frac{\lambda^2\left(n+\frac{N^2\Delta\xi^2}{2d'\lambda}\right)^2}{N^2\Delta\xi^2} - \frac{\lambda^2\left(m+\frac{N^2\Delta\eta^2}{2d'\lambda}\right)^2}{N^2\Delta\eta^2}}\right\}$

There is a conceptual difference between evaluation by the Fresnel transform using the chirp function as given in the first line of the table and the methods in the next four lines: If we take the (ξ, η)-plane of the digital hologram as the spatial domain, then the first mentioned procedure gives a result in the spatial frequency domain due to the single Fourier transform. The other four algorithms consist of a multiplication of the spectrum of $h \cdot r$ with a transfer function in the spatial frequency domain and a subsequent transform back into the spatial domain. A consequence of this difference is the dissimilarity of the pixel size in the reconstructed images (9) and (16). Despite the different magnitude it is remarkable that the size $\Delta x' \times \Delta y'$ in the Fresnel case using the chirp function (first line in the table) depends on the wavelength λ and the reconstruction depth d', while in the other four cases the size is independent of these parameters. This makes the latter algorithms especially useful if in-line holograms of scattering particles have to be evaluated in different depths. The sizes of all reconstructions agree and allow a direct comparison. No magnification for size adaptation with eventual interpolation is necessary. Experiments of that kind are described in detail in [10] in these proceedings.

In principle all mentioned methods are feasible for rendering the phase distributions in holographic interferometry. The two states of the object to be compared are recorded and evaluated individually. The phase distributions of the complex fields $b'_1(n,m)$ and $b'_2(n,m)$ are calculated, then their difference modulo 2π is produced which is the interference phase [1]. There is no remarkable difference in the interference phase distributions of the four methods based on the convolution approach. If the Fresnel transform is applied, only the size of the reconstructed image differs from those reconstructed by the convolution approach. This is demonstrated in Fig. 7. A plate was clamped at the edges and deformed by a central point load. The observable area was $130mm \times 80mm$. The wave field was reduced [7] by a lens of focal length $f = -100mm$ standing $710mm$ from the object surface. The lens had a distance of $432mm$ from the CCD-array that consisted of 2048×2048 pixels each $9\mu m \times 9\mu m$ large. Thus a virtual object of size $16mm \times 10mm$ appeared in a distance $d = 0.512m$ from the CCD. The wavelength was $\lambda = 0.6328\mu m$. The image size in the Fresnel evaluation now is $(d\lambda/\Delta\xi)^2 = (36mm)^2$, the interference phase distribution of this case is displayed in Fig. 7 a. The convolution approach gives an image size of $(N/\Delta\xi)^2 = (18.4mm)^2$, this result is shown

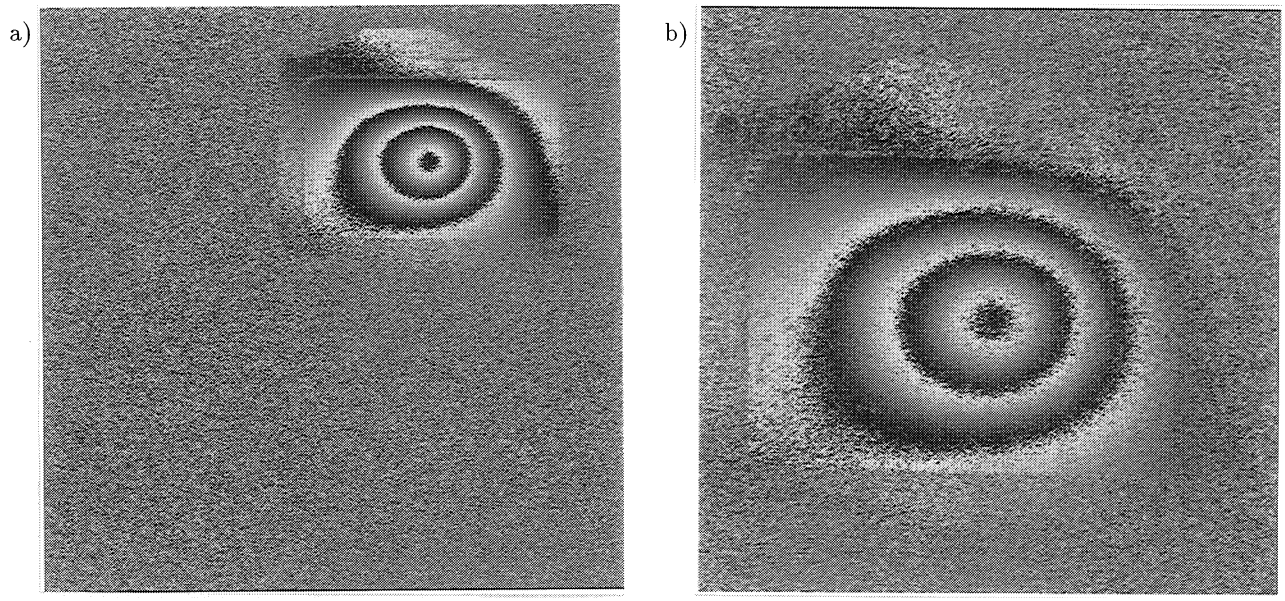

Figure 7: Interference phase distribution. Evaluation by Fresnel transformation (a) and by the convolution approach (b)

in Fig. 7 b. The smoother appearance of the interference phase in Fig. 7 a is a result of the inherent averaging effect in the production of the smaller image.

If small objects have to be investigated, at least theoretically we may work in a region where the Fresnel approximation of the spherical wavefronts by parabolic ones produces reasonable errors. Then the convolution approach is recommended since it yields an exact solution to the diffraction integral as far as the sampling theorem is not violated.

The last four algorithms in the table, where the inverse transform of the product in the spatial frequency domain is taken, yield identical results. However there are differences in the numerical treatment. In the calculation of the impulse response or the transfer function regions may occur where the argument of the complex exponential differs by more than π between adjacent pixels. At these points the absolute value of the calculated impulse response or transfer function has to be set to zero. It can be proven that for large d' the impulse response is defined at many pixels, but the transfer function only at a few. Conversely for small d' the transfer function is defined at many pixels, the impulse response only at a few. This performance is also realized by the Fourier transform that maps the impulse response onto the transfer function and vice versa. Thus the result is independent from the choice of the specific reconstruction algorithm among the mentioned four.

6 CONCLUSIONS

Digital recording and numerical reconstruction of holograms offer new possibilities to optical metrology. The numerical evaluation of digital Fresnel holograms can be performed by the Fresnel transform or by a convolution corresponding to the diffraction integral. The main difference in the results of these two approaches is in the size of the pixels in the reconstructed image. Therefore if reconstructions in different depths are to be compared, as in the measurement of scattering particles by in-line holography, the convolution approach is recommended, because here the size of the image does not depend on the reconstruction depth. If the whole possible field of view for opaque or transparent objects has to be reconstructed, the Fresnel transform is the best choice.

ACKNOWLEDGEMENTS

The described fundamental research was sponsored by the German Research Council (Deutsche Forschungsgemeinschaft DFG) under grant Kr 953/12, while the practical applications in in-line holography for particle analysis were funded in the DFG-Sonderforschungsbereich 372: Sprühkompaktieren (Spray Forming) which is gratefully acknowledged.

References

[1] Th. Kreis. *Holographic Interferometry: Principles and Methods*, Akademie-Verlag, Berlin, and VCH Publishers, Inc., New York, 1996.

[2] A. Macovski, S. D. Ramsey, and L. F. Schaefer. Time-lapse interferometry and contouring using television systems. Appl. Opt., 10, 2722–2727, 1971.

[3] J. N. Butters and J. A. Leendertz. Holographic and video techniques applied to engineering measurements. Meas. and Contr., 4, 349–354, 1971.

[4] U. Schnars. Direct phase determination in hologram interferometry with use of digitally recorded holograms. J. Opt. Soc. Amer. A, 11, 2011–2015, 1994.

[5] U. Schnars and W. P. O. Jüptner. Direct recording of holograms by a CCD target and numerical reconstruction. Appl. Opt., 33(2), 179–181, 1994.

[6] G. Pedrini, Y. L. Zou, and H. J. Tiziani. Digital double-pulsed holographic interferometry for vibration analysis. J. Mod. Opt., 42(2), 367–374, 1995.

[7] U. Schnars, Th. M. Kreis, and W. P. O. Jüptner. Digital recording and numerical reconstruction of holograms: reduction of the spatial frequency spectrum. Opt. Eng., 35(4), 977–982, 1996.

[8] J. W. Goodman. *Introduction to Fourier Optics*, McGraw-Hill Companies, Inc., New York, Second Edition 1996.

[9] Th. Kreis, and W. Jüptner. The suppression of the d.c.-term in digital holography. To appear in Opt. Eng., 36, 1997.

[10] M. Adams, Th. Kreis, and W. Jüptner. Particle size and position measurement with digital holography. Proc. of European Symposium on Lasers and Optics in Manufacturing, SPIE, 1997.